
MIDB atlas: A precision functional atlas of personalized network topography and probabilities

Robert J. M. Hermosillo, Lucille A. Moore, Eric Feczko, Óscar Miranda-Domínguez, Adam Pines...

DOI: 10.1038/s41593-024-01596-5

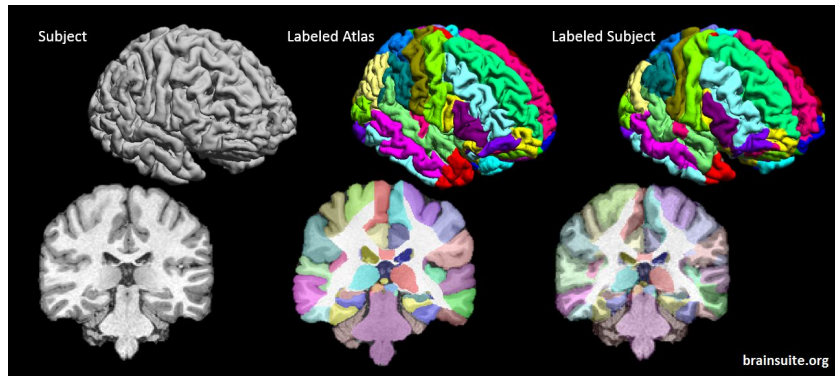
Review article

Nature Neuroscience

Online: 26 March 2024

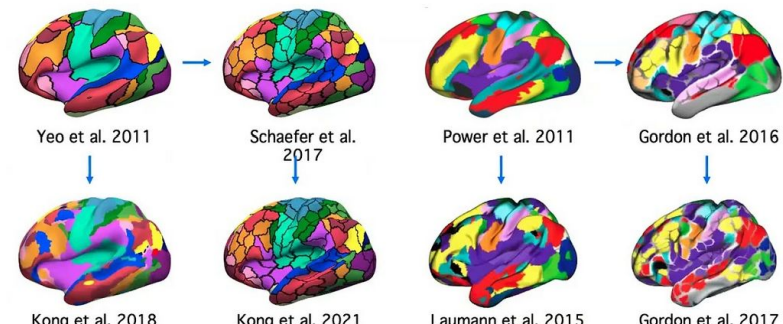
Codes publicly available at <https://github.com/DCAN-Labs>
<https://midbatlas.io/>

Context: topography variability of functional neural networks



Structural probabilistic atlas

Individual-specific Network-level Parcellation



Functional probabilistic atlases (OHBM 2022)

<https://www.youtube.com/watch?app=desktop&v=eFS2G6xGwSk>

- Precision Functional Mapping (Laumann et al., 2015): 14h of resting-state fMRI data
 - ↳ specific aspects of the topographical neural organization highly unique
- Probabilistic atlases historically structural and not functional:
 - probabilistic weights to attempt to delineate anatomical structures
 - probabilistic volumes for subcortical structures
- Functional probabilistic maps:
 - could be used for individual-specific functional mappings with improved reproducibility
 - could enhance neuronavigation for targeted brain stimulation

Work here: new methods of network identification

- **Infomap (IM)**: Information theory (Huffman coding) to map networks by modeling the flow between nodes.
- **Template matching (TM)**: assigns each grayordinate to a network by comparing the whole-brain connectivity of the grayordinate to a series of network templates observed in the group (Gordon et al., 2017)
- **Non-negative matrix factorization (NMF)**:
- **Overlapping MultiNetwork Imaging (OMNI) mapping**: data-driven approach to assign multiple networks to each grayordinate. Use local minimum of the characteristic skewed bimodal distribution of η_2 values as threshold to assign a specific network. As a consequence, grayordinates are not preferentially linked to any given network and can be unassigned.

Datasets

- **Main dataset:** ABCD (Adolescent Brain Cognitive Development)
 - supported by NIH (National Institutes of Health)
 - 11,987 US children, starting at 9-10 yo, and then biennially for 10 years
 - 20 min rs-fMRI (resting-state functional MRI), 3-4 mm resolution at 3T
 - 40 min t-fMRI (task)
 - BOLD signal (blood-oxygen-level-dependent signal, fNIRS), $1 \times 1 \times 2$ mm resolution
 - ↳ providing enough for producing individual functional network mapping
- Additional maps across additional ages:
 - HCP-D (Lifespan Human Connectome Project Development)
 - Dartmouth dataset
 - Washington University dataset
 - Midnight Scan Club (MSC) dataset

Datasets

Dataset	N (N female)	Average age (years)	Usage	HCP-D ages 14-15 ³	84	15.0	Probabilistic maps and ROI sets provided
MSC ⁴	10 (5)	29.3	Within-subject reliability testing, probabilistic maps provided.	HCP-D ages 16-17 ³	59	16.9	Probabilistic maps and ROI sets provided
ABCD group1 ⁵ test group	2995 ()	9.9	Generating probabilistic maps, used in brain -behavior reliability analysis. used for the creation of integration zones used to make probabilistic ROIs.	HCP-D ages 18-19 ³	52	18.9	Probabilistic maps and ROI sets provided
ABCD group2 ⁵ test group	3111	9.9	Generating probabilistic maps, used in brain -behavior reliability analysis. used for the creation of integration zones	HCP-D ages 20-21 ³	67	21.0	Probabilistic maps and ROI sets provided
ABCD group3 ⁵ Network templates for TM	163	9.8	Used to make the network template for template matching.	HCP-D ages 08-13	81	11.45	Correlation between probabilistic maps for broader age ranges.
ABCD test cohort	10	9-10	Within-subject reliability	HCP-D ages 08-13	81	11.49	Correlation between probabilistic maps for broader age ranges.
HCP-D ages 8-9 ³	38	9.2	Probabilistic maps and ROI sets provided	WashU-120 ³⁵	130	25.0	Group-average for data-driven discovery cohort, probabilistic maps provided
HCP-D ages 10-11 ³	53	10.9	Probabilistic maps and ROI sets provided	Dworetzky-Dartmouth ²⁵	69	20.2	Probabilistic maps and ROI sets provided
HCP-D ages 12-13 ³	72	13.1	Probabilistic maps and ROI sets provided	Dworetzky-HCP ²⁵	384	28.4	Probabilistic maps and ROI sets provided
				Dworetzky-Yale ²⁵	65	32.3	Probabilistic maps and ROI sets provided
				MIDB subpopulation	5	9-10	Within-subject reliability testing

Datasets

Extended Data Table 3 | Group demographics table—participants with at least 10 min of resting-state data

Variable	Group1 (N=2995)	Group2 (N=3111)	Group3 (N=161)
	mean (sd)	mean (sd)	mean (sd)
Age (in months)	119.64 (7.48)	119.75 (7.47)	118.37 (7.73)
Grade level	4.27 (0.78)	4.27 (0.78)	4.20 (0.76)
Highest parent education	17.38 (2.85)	17.34 (2.46)	16.83 (2.90)
Combined income (in thousands).	7.51 (2.24)	7.46 (2.24)	7.08 (2.35)
<hr/>			
categorical	Group1 (N=2995)	Group2 (N=3111)	Group3 (N=161)
	count (%)	count (%)	count (%)
# Female*	1411 (47.10)	1544 (49.66)	78 (48.45)
Anesthesia exposure	966 (32.2)	1005 (32.3)	42 (26.1)
Right handed	2401 (80.2)	2525 (81.2)	136 (84.5)
<hr/>			
Race/Eth			
White	2399 (80.10)	2460 (79.07)	106 (65.84)
Black	539 (18.00)	556 (17.87)	30 (18.63)
AI/AK**	94 (3.14)	99 (3.18)	4 (2.48)
NHPI	19 (0.63)	18 (0.58)	0(0)
Asian	62 (2.07)	62 (1.99)	6 (0.373)
Other	143 (4.77)	166 (5.34)	21 (13.04)
Unknown	23 (0.77)	34 (1.09)	4 (2.48)
Latinx	544 (18.16)	564 (18.13)	28 (17.39)
<hr/>			
site	Group1 (N=2995)	Group2 (N=3111)	Group3 (N=161)
	count (%)	count (%)	count (%)
1	41 (1.37)	49 (1.58)	4 (2.48)
2	212 (7.08)	205 (6.59)	9 (5.59)
3	199 (6.64)	213 (6.85)	5 (3.11)
4	205 (6.84)	182 (5.85)	9 (5.59)
5	103 (3.44)	112 (3.60)	12 (7.45)
6	170 (5.68)	170 (5.46)	22 (13.66)

TM results

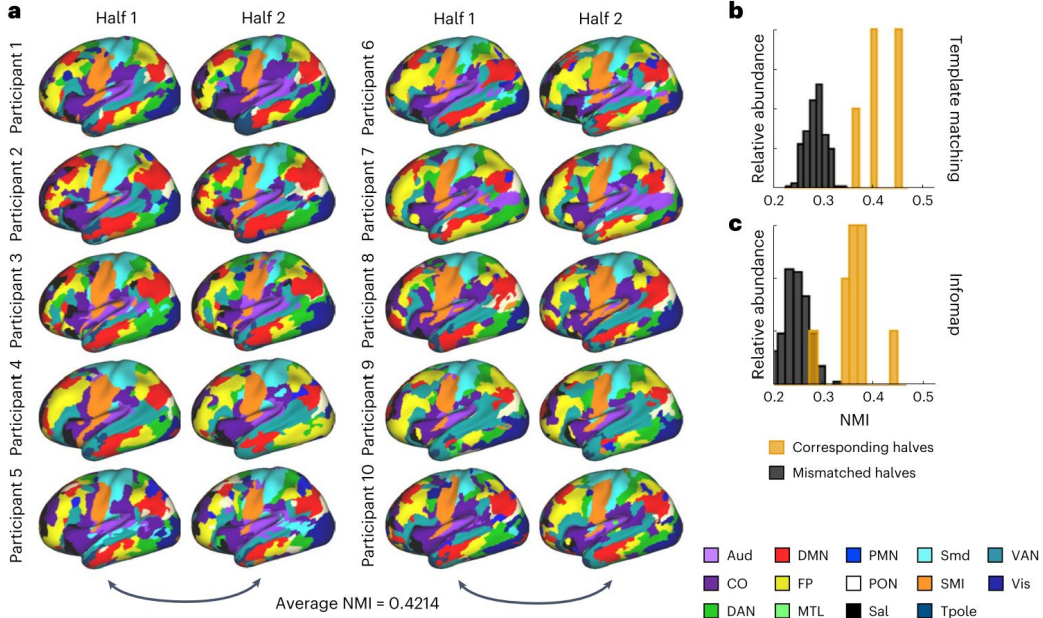


Fig. 1 | Example of precision maps of ABCD participants using TM. **a**, Example of networks determined by the TM procedure for participants with at least 20 min of low-motion resting-state data. Resting-state time series were split in half, and networks were obtained for each half ($n = 10$). Only the left hemisphere is shown for visualization purposes, but networks were also identified in the

right hemisphere, subcortex and cerebellum. **b**, The NMI was calculated between participants' own halves (gold bars) and others in the split-half group (gray bars) using TM. **c**, We also generated network maps using the IM procedure and performed an identical NMI comparison.

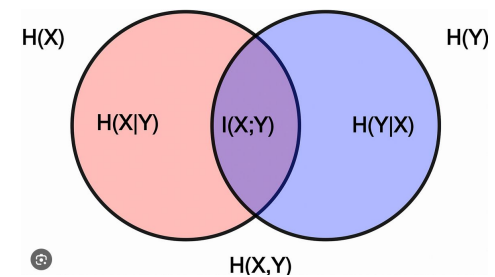
5.2.2 Normalized mutual information

NMI is a popular information theory measure used to evaluate the clustering quality. If we have two random variables \mathbf{X} and \mathbf{Y} , the NMI between them is computed as follows:

$$NMI(\mathbf{X}, \mathbf{Y}) = \frac{I(\mathbf{X}, \mathbf{Y})}{\sqrt{H(\mathbf{X})H(\mathbf{Y})}}, \quad (21)$$

where $I(\mathbf{X}, \mathbf{Y})$ is the mutual information between \mathbf{X} and \mathbf{Y} ; $H(\mathbf{X})$ and $H(\mathbf{Y})$ are the entropies of \mathbf{X} and \mathbf{Y} , respectively. The mutual information between \mathbf{X} and itself is 1. The larger the NMI, the better the performance. Specifically, NMI can be computed as

$$NMI = \frac{\sum_{l=1}^c \sum_{h=1}^c n_{l,h} \log(\frac{n \times n_{l,h}}{n_l \hat{n}_h})}{\sqrt{(\sum_{l=1}^c n_l \log \frac{n_l}{n})(\sum_{h=1}^c \hat{n}_h \log \frac{\hat{n}_h}{n})}}, \quad (22)$$



Network probability

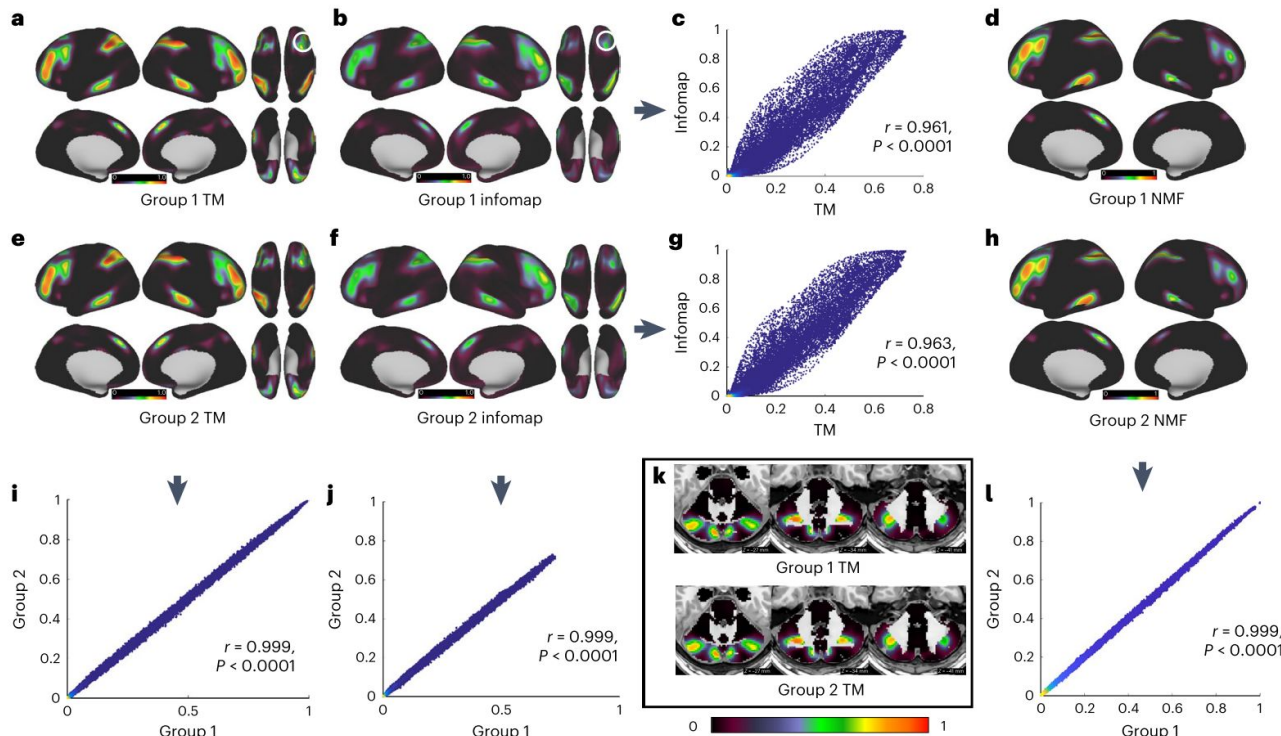


Fig. 2 | Example of network probability. **a,b,d–f,h**, An example of network probability for the frontoparietal network using TM (**a,e**), IM (**b,f**; surface only) and NMF (**d,h**; surface only) procedures with single network assignment. **i,j,l**, The between-group correlation for TM (**i**), IM (**j**) and NMF (**l**), respectively. **c,g**, The correlation between methods for ABCD-group 1 (**c**) and ABCD-group 2 (**g**), respectively. For additional probability maps, see Supplementary Fig. 8.

k, Network probabilistic map for the frontoparietal network within the cerebellum. White circles in **a** and **b** highlight similar probabilistic functional asymmetries in the SMA across methods. Each dot in **c**, **g**, **i**, **j** and **l** represents one grayordinate. Independent Pearson's correlations were conducted between groups 1 and 2 for each network. The color in the scatterplot is the probability density estimate based on a normal kernel function. SMA, supplementary motor area.

Comparing connectivity

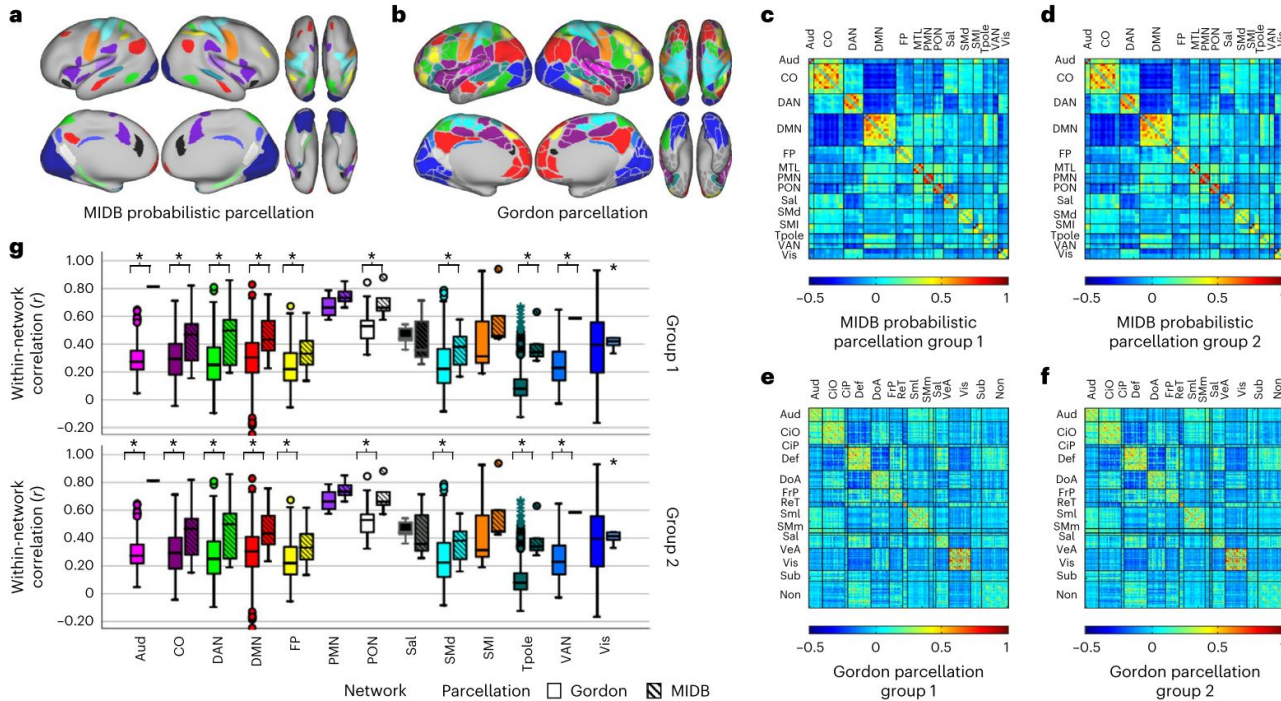


Fig. 3 | Comparing connectivity using probabilistic ROIs and Gordon ROIs.
a, MIDB probabilistic parcellation (75% probability of network consensus using the TM). **b**, Gordon parcellation. Parcels are colored according to network assignment. Similar colors were used between parcellations where possible. **c–f**, Connectivity matrices were generated using the MIDB probabilistic parcellation (**c,d**) and the Gordon parcellation (**e,f**) for ABCD-group 1 (**c,e**) ($n = 2,995$) and ABCD-group 2 (**d,f**) ($n = 3,111$). **g**, In total, 9 of 13 shared networks showed significantly higher within-network connectivity in the MIDB probabilistic parcellation compared to the Gordon parcellation. Open boxes represent Gordon parcellation; striped boxes represent MIDB probabilistic parcellation. t tests were conducted between methods using within-network

connections using group average connectivity matrices (Aud, d.f. = 275; CO, d.f. = 844; DAN, d.f. = 522; DMN, d.f. = 896; FP, d.f. = 276; PMN, d.f. = 14; PON, d.f. = 32; Sal, d.f. = 19; SMD, d.f. = 716; SMI, d.f. = 32; Tpole/unlabeled, d.f. = 1079; VAN, d.f. = 252; Vis, d.f. = 745; the number of ROIs and therefore the number of degrees of freedom are identical for groups 1 and 2). $*P < 0.05$ (Benjamini-Hochberg corrected, two-tailed). Boxplots show median and IQR (box size). The maximum and minimum whiskers represent $Q3 + 1.5 \times IQR$ and $Q1 - 1.5 \times IQR$. IQR, interquartile range; CiO, cingulo opercular; CiP, cingulo parietal; Def, default; DoA, dorsal attention; FrP, frontoparietal; ReT, retrosplenial temporal; Sml, somatomotor lateral; SMm, somatomotor medial; VeA, ventral attention; Sub, subcortical; Non, no assignment.

MIDB probabilistic parcellation compared to Gordon parcellation

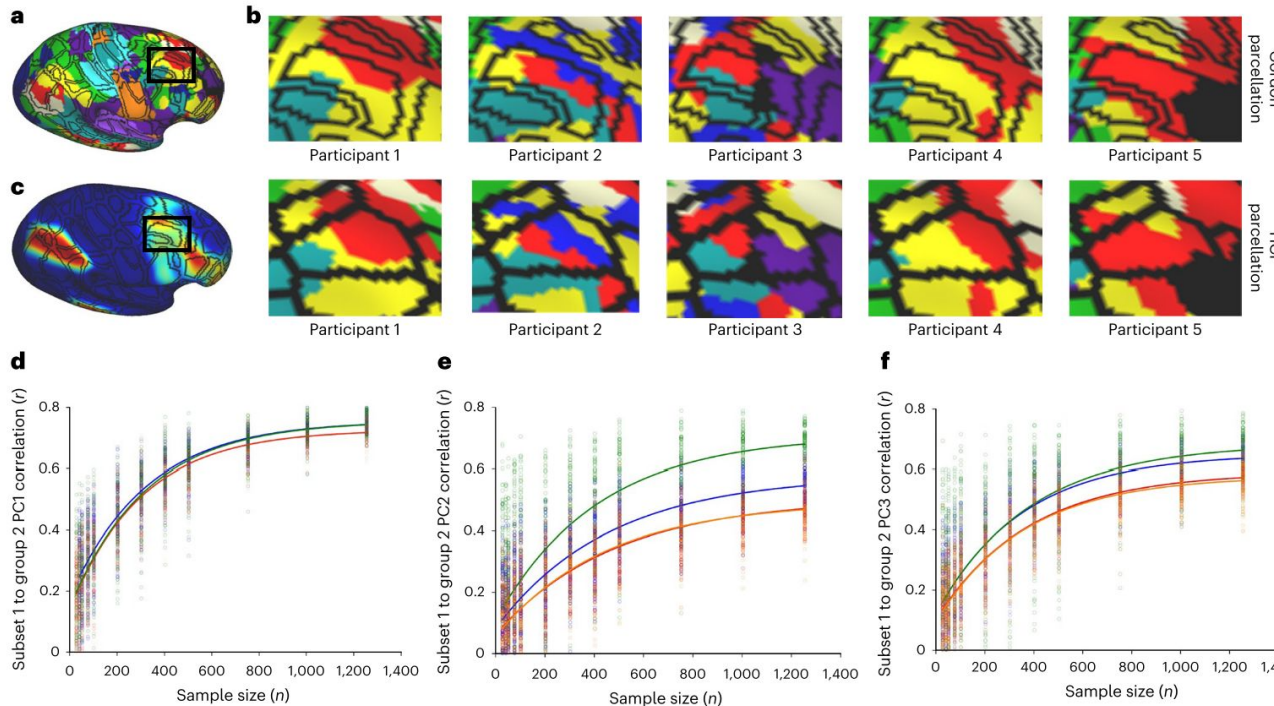


Fig. 4 | Neural networks have unique topographies that confound conventional ROI sets. The black lines indicate the boundaries of the parcels. **a**, The dorsolateral aspect of the frontal lobe demonstrates that parcels may belong to one of several potential networks. **b**, An example of ten individuals' neural networks with the Gordon parcellation (top row) and HCP parcellation (bottom row) overlaid. Frontoparietal is shown as yellow. **c**, The frontoparietal probabilistic map indicates inhomogeneity in network topography among the population. **d–f**, Subset reliability analysis showing that using the MIDB probabilistic parcellation improves signal-to-noise in group-level predictions

relative to the Gordon parcellation. Blue circles/lines indicate intergroup correlation for each random subset using the MIDB probabilistic parcellation. Red circles/lines indicate intergroup correlation for each random subset using the Gordon parcellation. Green circles/lines indicate intergroup correlation for each random subset using the integration zone parcellation. Orange circles/lines indicate intergroup correlation for each random subset using 80 randomly selected parcels from Gordon parcellation. Data were fitted with an exponential rise-to-maximum equation. Please note red and orange fitted curves are nearly identical, which obscures visual discernment.

OMNI mapping

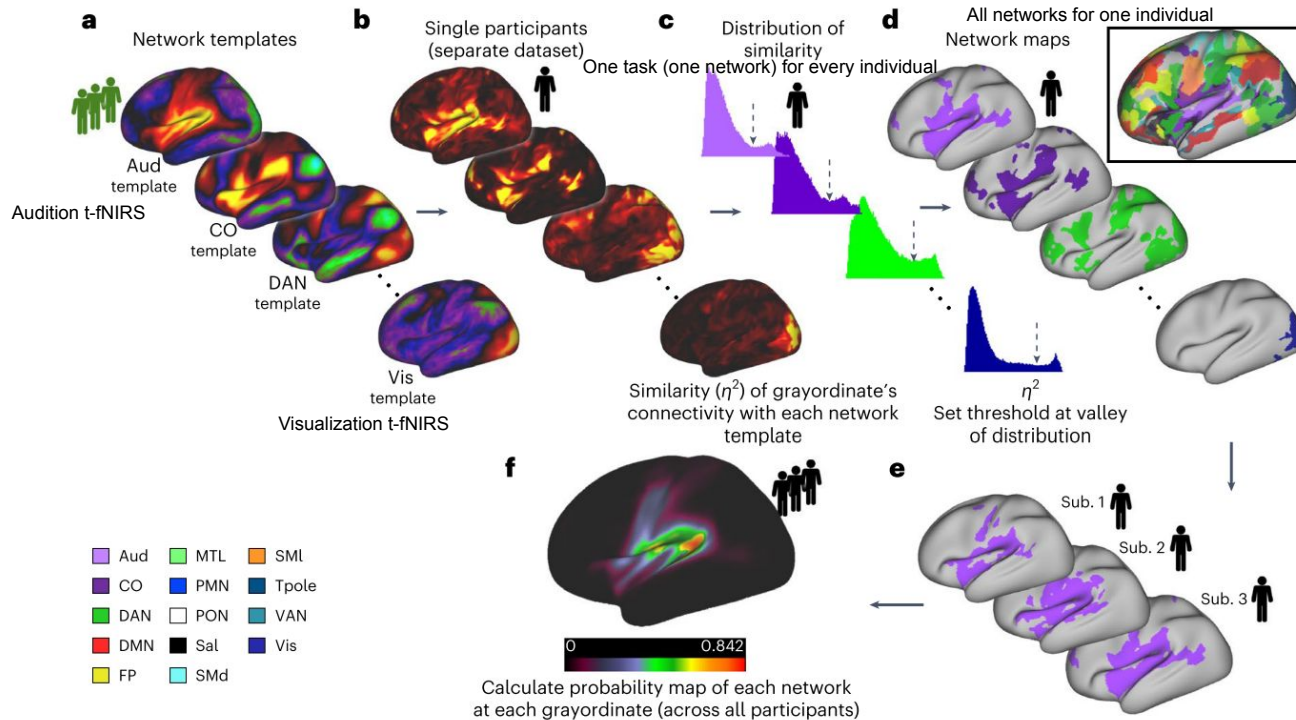


Fig. 5 | Method for detecting overlapping networks using OMNI mapping.
a, A series of network templates were generated using an independent group of participants (ABCD-group 3). **b**, For each participant, the similarity at each grayordinate (using η^2) was calculated to each of the network templates shown in **a**. **c**, We set a threshold (dashed arrow) for each network, based on the observed

local minimum between peaks of bimodal distribution of η^2 . **d**, Grayordinates that had η^2 values that were above the threshold were then assigned that network label. All overlapping networks for an example participant are shown in the inset. **e,f**, After this procedure is performed for all participants, we calculate a probabilistic map for each network (only the Aud is shown).

Results across ages

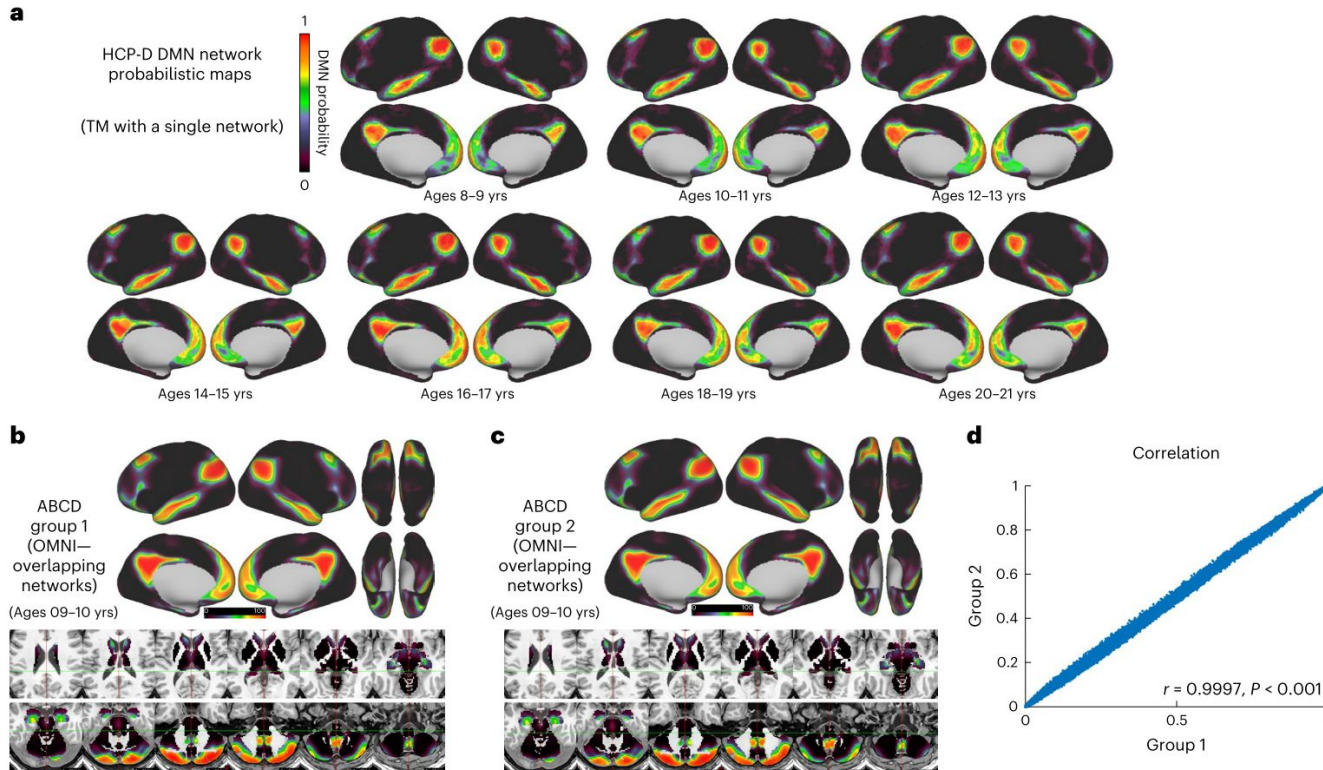


Fig. 6 | Probabilistic map consistency across ages. **a**, Probabilistic maps from adolescence to adulthood. Here we show the DMN probabilistic map. Please note additional probabilistic maps are available for additional age groups from the HCP-D study (<https://midbatlas.io/>). **b–d**, Network probability maps using OMNI mapping. At each grayordinate, the probability of observing each network

was calculated for ABCD-group 1 and ABCD-group 2. Here the DMN is shown as an example. **d**, The correlation of the probability maps depicted in **b** and **c** (excluding zeros; mismatched zeros = 0.033%). See Supplementary Fig. 9 for additional networks.

Multiple overlapping networks

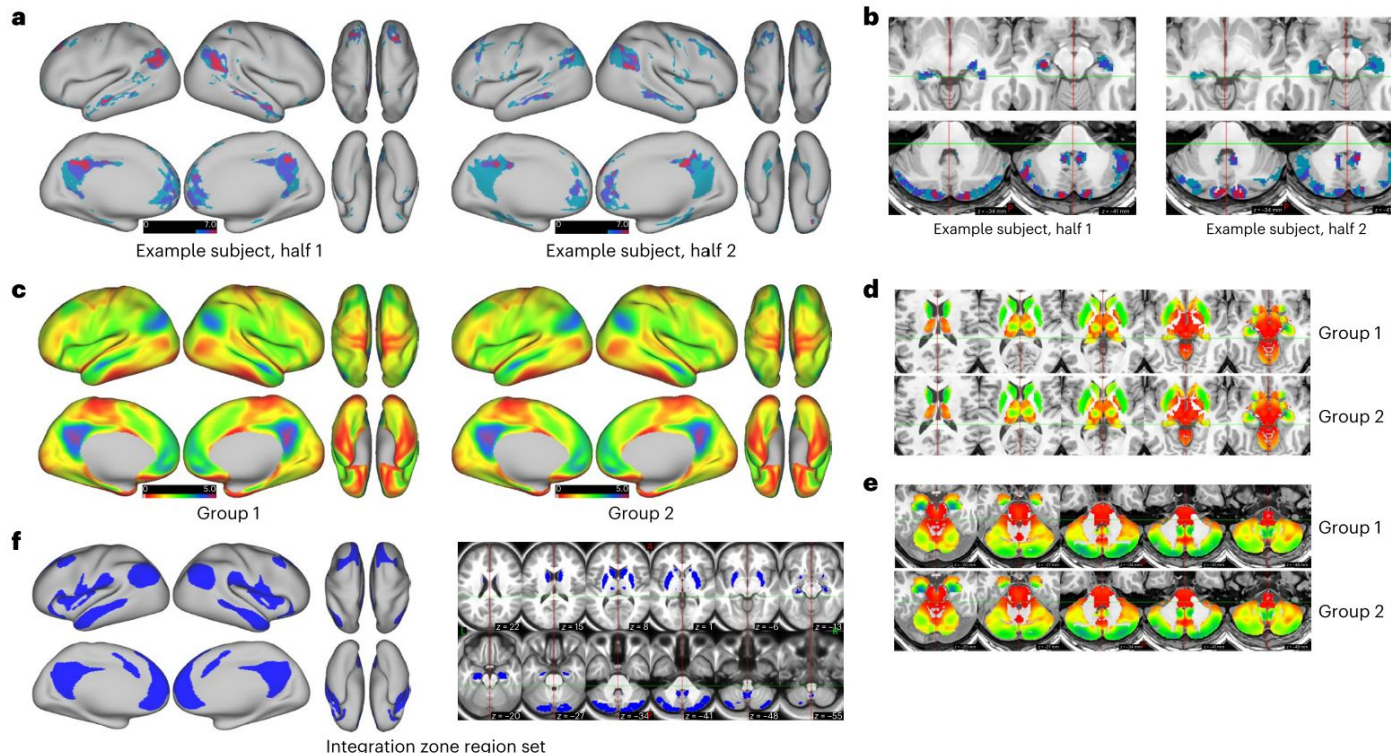


Fig. 7 | Identifying regions with multiple overlapping networks using OMNI mapping. **a,b**, An example of regions identified on the cortex, subcortical nuclei (**a**) and cerebellum that have five or more networks overlapping in an individual participant (image has been thresholded for visualization purposes) (**b**). **c–e**, The number of networks that overlap at each grayordinate for ABCD-group

1 and ABCD-group 2. The hippocampi and the posterior cerebellum (in particular the spinocerebellum) also demonstrate high network overlap. **f**, Brain-wide maps of the average number of overlapping networks for ABCD-group 1 (shown in **c**) were thresholded at 2.2 networks to generate an integration zone region set.

Thank you for your attention

Context: topography variability of functional neural networks

Context: topography variability of functional neural networks

- Set of precision functional network atlases: Masonic Institute for the Developing Brain (MIDB)
 - Ressources: 53273 individual-specific network maps from more than 9900 individuals (across ages and cohorts)
 - Probabilistic network maps across multiple ages and integration wones (using Ovelapping MultiNetwork Imaging)
 - Improve reproducibility of executive function statistical maps
 - Using probabilistic maps for targeted neuromodulation

Context: topography variability of functional neural networks

But in medical imaging...

Challenges:

- Significant differences between image modalities (3D/2D), imaging protocols and machines, etc.
- Segmentation task can vary depending on the specific clinical scenario
 - (Example: segmenting the liver tumor VS entire liver and surroundings organs on CT scan)
 - Need of user provided prompts

MedSAM training and validation method

Fine-tuning SAM with:

- **1,570,263 image-mask pairs** (unprecedented dataset; 80% training, 10% tuning, and 10% validation)
 - MRI/CT slices in **NifTI format** + [0, 255] intensity normalization + [1024×1024×3] resizing
 - Grayscale/RGB in **png format** + [1024×1024×3] resizing
- **10 images modalities**, with a multitude of imaging protocols
- **30 cancer types**
- **86 internal validation tasks**
- **60 external validation tasks**
 - Unseen segmentation targets
 - New domains (cell segmentation in LM images and organelle segmentation in EM images)

Comparison with:

- SOTA segmentation foundation model **SAM**
- 10 dedicated specialist models based on **U-Net** and **DeepLabV3+** respectively

MedSAM datasets distribution and MedSAM architecture

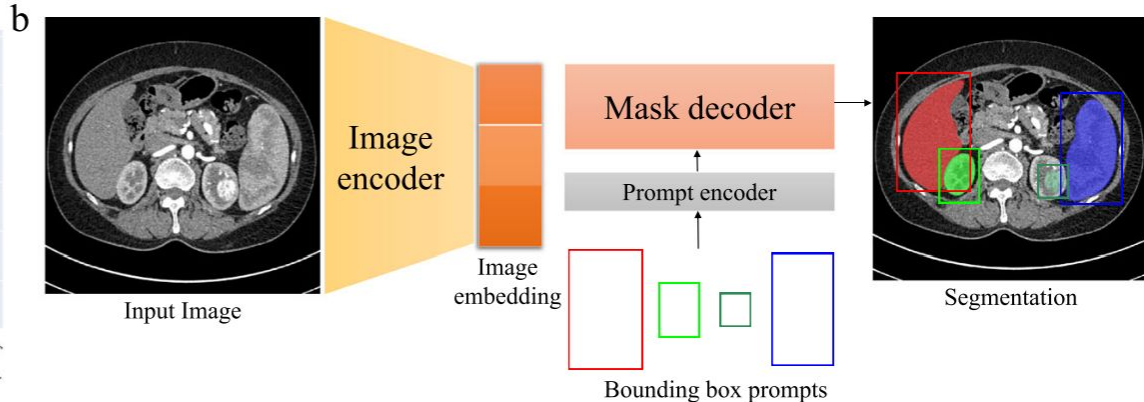
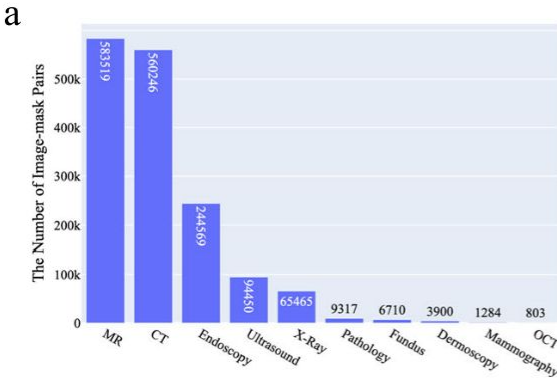


Fig. 2 | Overview of the modality distribution in the dataset and the network architecture. a The number of medical image-mask pairs in each modality. b MedSAM is a promptable segmentation method where users can use bounding boxes to specify the segmentation targets. Source data are provided as a Source Data file.

TABLE 5

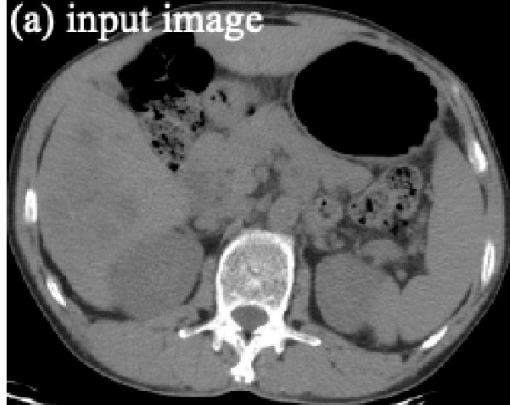
The number of training images for modality-wise specialist models.

Modality	Num. of Training Images
Computed Tomography	362,229
Magnetic Resonance Imaging	442,818
X-Ray	36915
Mammography	986
Optical Coherence Tomography	642
Ultrasound	74761
Dermoscopy	2955
Endoscopy	194805
Fundus	960
Pathology	6239

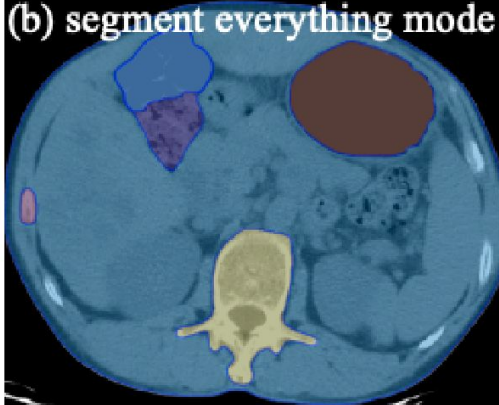
- **Image encoder based on vision transformer:**
 - 12 transformer layers
 - multi-head self-attention and multilayer perceptron per block
- **Mask decoder:**
 - feature size in image embedding of 64×64

MedSAM prompt types

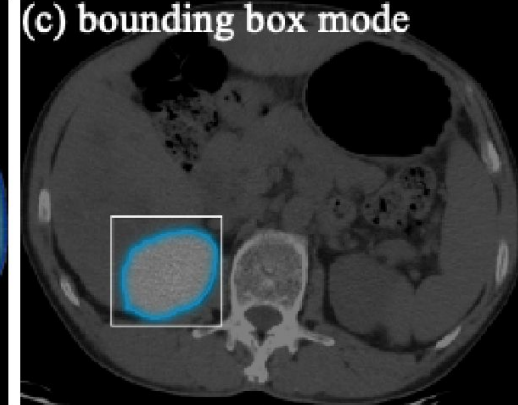
(a) input image



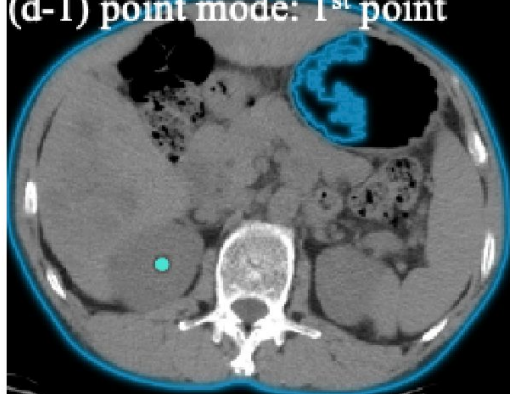
(b) segment everything mode



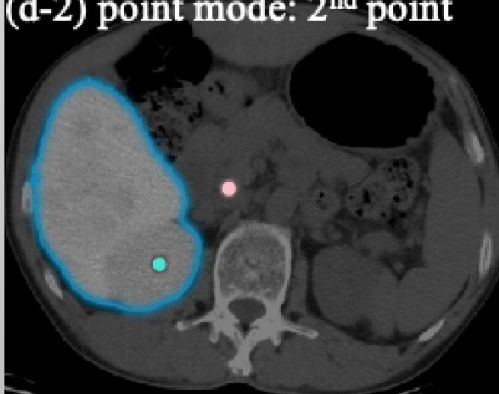
(c) bounding box mode



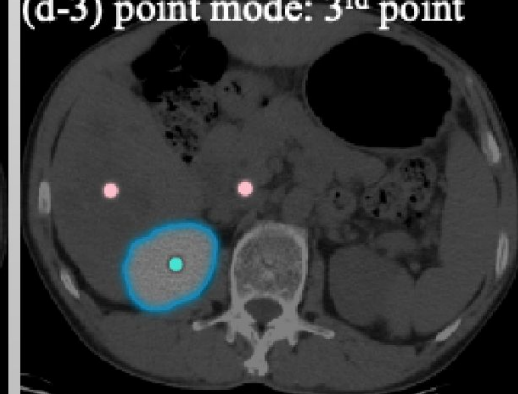
(d-1) point mode: 1st point



(d-2) point mode: 2nd point



(d-3) point mode: 3rd point



MedSAM Loss function

Binary cross entropy loss:

$$L_{\text{BCE}} = -\frac{1}{N} \sum_{i=1}^N [g_i \log s_i + (1 - g_i) \log(1 - s_i)]$$

Dice loss:

$$L_{\text{Dice}} = 1 - \frac{2 \sum_{i=1}^N g_i s_i}{\sum_{i=1}^N (g_i)^2 + \sum_{i=1}^N (s_i)^2}$$

Total loss:

$$L = L_{\text{BCE}} + L_{\text{Dice}}$$

si, gi denotes the predicted segmentation and ground truth of voxel i, respectively.

N is the number of voxels in the image I.

MR image datasets

TABLE 2

Magnetic Resonance (MR) image datasets. Datasets marked with * denote external validation sets and the remaining datasets are used for internal validation.

Dataset Name	Modality	Segmentation Targets	# of scans	
ACDC* [30]	MR	Heart anatomies	150	https://humanheart-project.creatis.insa-lyon.fr/
AMOS-MR [6]	MR	Abdominal organ	40	https://amos22.grand-challenge.org/Dataset/
ATLAS R2.0 [31]	MR-T1	Brain stroke	1271	https://atlas.grand-challenge.org/
Brain Tumor Dataset Figshare [32], [33]	MR-T1ce	Brain tumor	233	https://www.kaggle.com/datasets/ashkhagan/
Brain TR-GammakKnife [34]	MR	Brain lesion	47	https://doi.org/10.7937/x6d-py67
BraTS [35]–[39]	MR-T1, MR-T1CE, MR-T2, MR-FLAIR	Brain tumor	1251	http://braintumorsegmentation.org/
CC-Tumor Heterogeneity* [40]	MR	Cervical cancer	7	https://doi.org/10.7937/ERZ5-QZ59
CHAOS* [41]	MR-T1, MR-T2	Liver, kidney, spleen	60	https://chaos.grand-challenge.org/
crossMoDA [42]	MR	Brain tumor	227	https://crossmoda-challenge.ml/
FeTA [42]	MR-Fetal	Brain tissues	160	https://feta.grand-challenge.org/
HaN-Seg* [43]	MR	Head organs	42	https://zenodo.org/record/
ISLES [44]	MR-DWI, MR-ADC, MR-FLAIR	Ischemic stroke lesion	180	http://www.isles-challenge.org/
I2CVB [45]	MR-T2, MR-DWI	Prostate	19	https://i2cvb.github.io/
Meningioma-SEG-CLASS [46]	MR-T1ce, T2-FLAIR	Tumor (meningioma)	191	https://doi.org/10.7937/0TKV-1A36
MMs [47]	MR	Heart anatomies	150	https://www.ub.edu/mnms-2/
MSD-Heart [48]	MR	Left atrial	30	http://medicaldecathlon.com/
MSD-Prostate [21]	MR-ADC, MR-T2	Prostate	48	http://medicaldecathlon.com/#tasks
NCI-ISBI [49]	MR-ADC, MR-T2	Prostate	48	http://dx.doi.org/10.7937/K9/TCIA.2015.zF0vl
PI-CAI [50]	MR-bp	Prostate cancer	1584	http://github.com/DIAGNijmegen/picai_labels
PPMI [51]	MR-T1	Brain regions of Parkinson patients	1130	https://www.ppmi-info.org/access-data-specim
PROMISE [52]	MR-T2	Prostate	50	https://promise12.grand-challenge.org/Details
Qin-Prostate-Repeatability [21], [53]	MR	Left atrium	30	http://doi.org/10.7937/K9/TCIA.2018.MRICKO
QUBIQ* [54]	MR	Prostate	52	https://qubiq21.grand-challenge.org/
Spine [55]	MR	Vertebrae	172	https://www.cg.informatik.uni-siegen.de/en/spine.html
WMH [56]	MR-T1, MR-FLAIR	White matter hyper-intensities	60	https://wmh.isi.uu.nl/

Evaluation metrics

$$\text{DSC}(G, S) = \frac{2|G \cap S|}{|G| + |S|}$$

Dice similarity coefficient: evaluate the region overlap between expert annotation masks and segmentation results

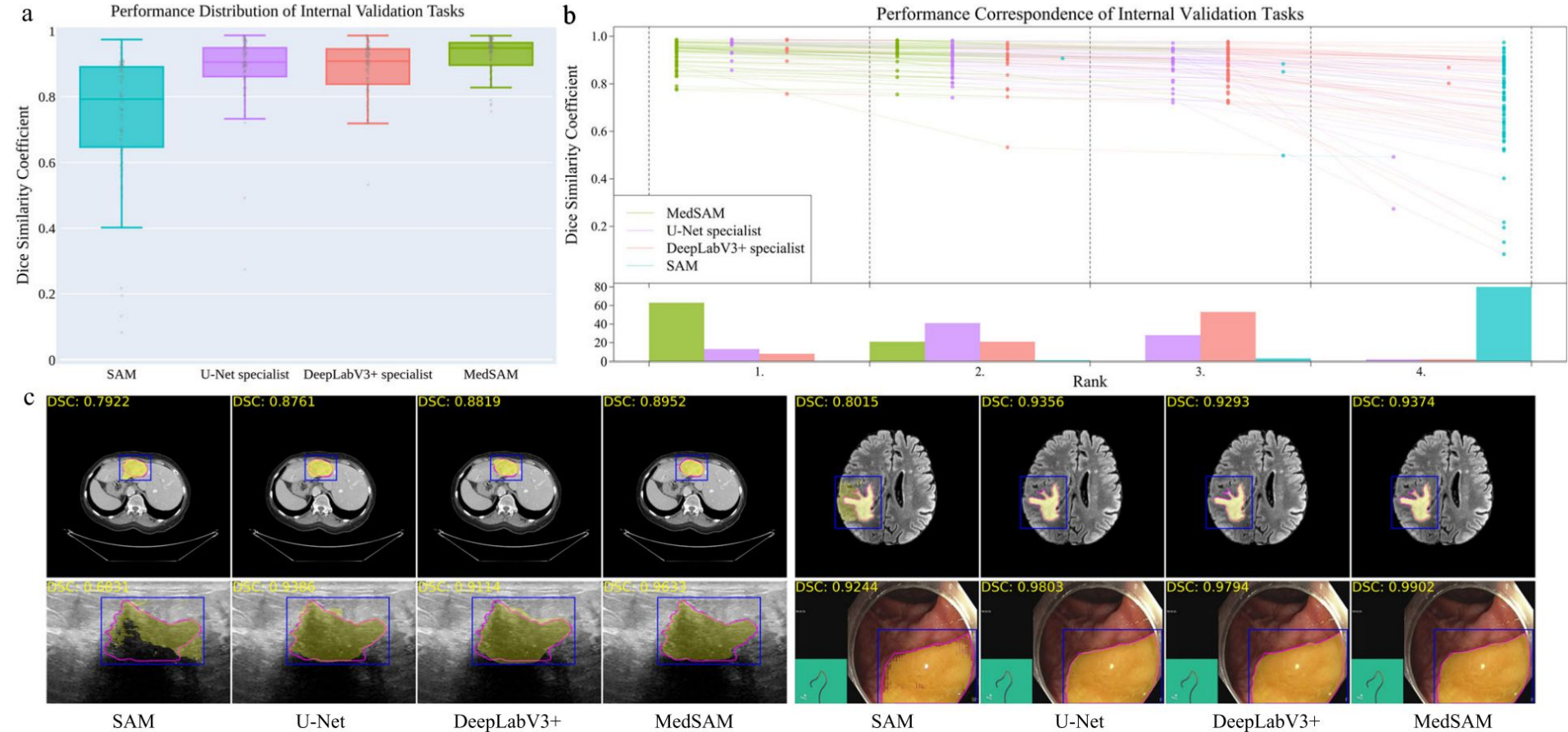
$$\text{NSD}(G, S) = \frac{|\partial G \cap B_{\partial S}^{(\tau)}| + |\partial S \cap B_{\partial G}^{(\tau)}|}{|\partial G| + |\partial S|}$$

Normalized surface distance: evaluate the boundary consensus between expert annotation masks and segmentation results at a given tolerance

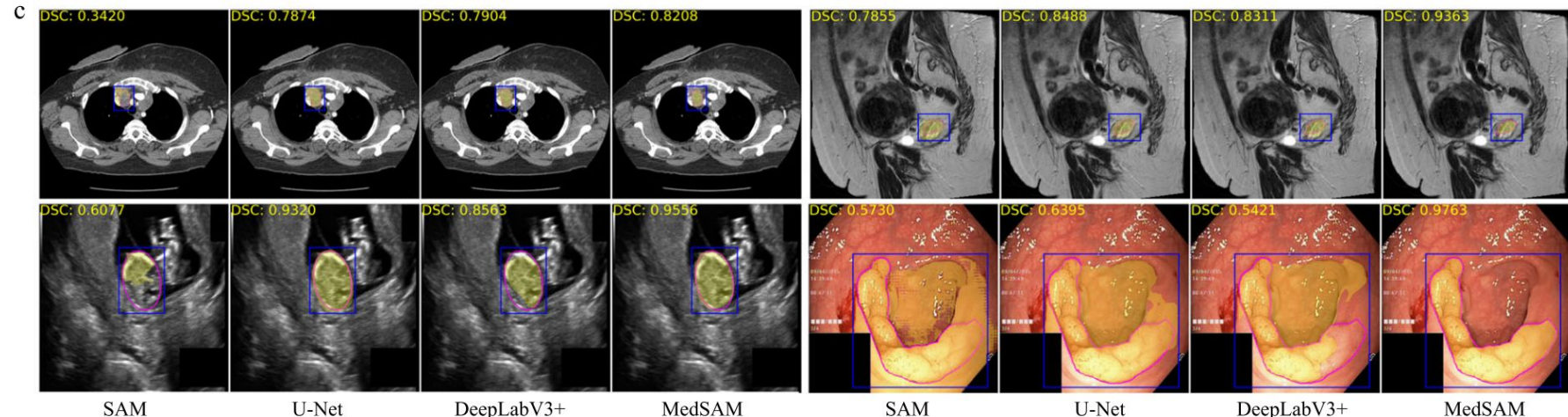
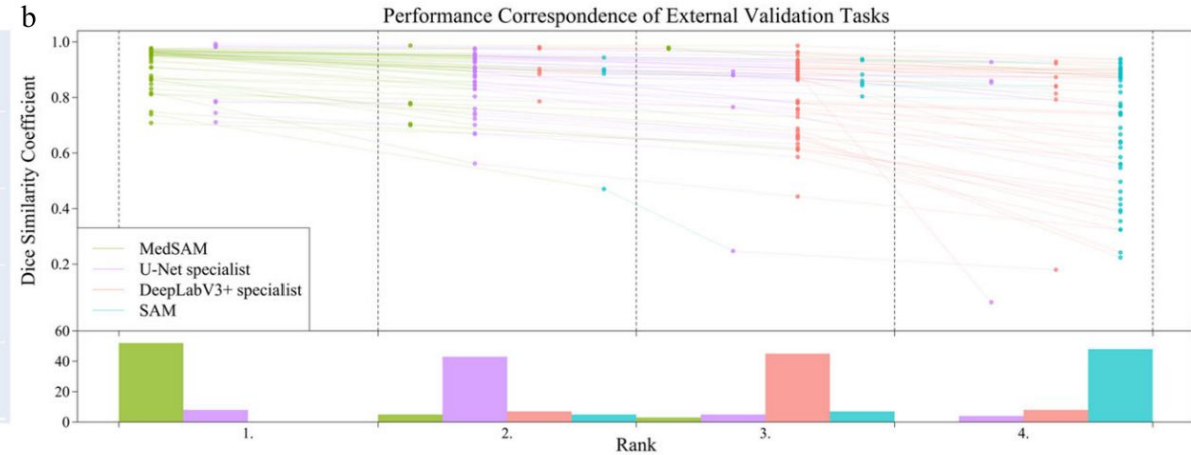
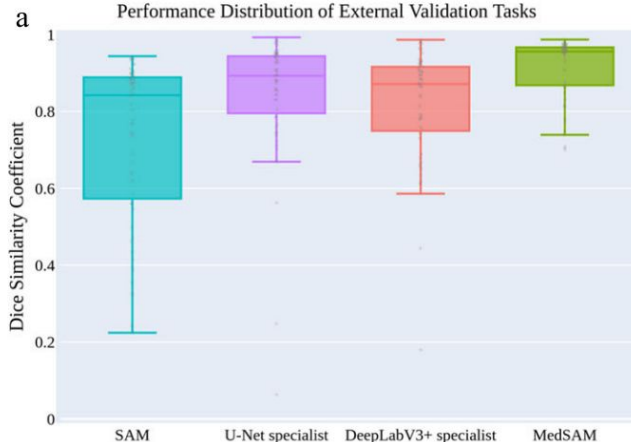
where $B_{\partial G}^{(\tau)} = \{x \in R^3 \mid \exists \tilde{x} \in \partial G, \|x - \tilde{x}\| \leq \tau\}$,

$B_{\partial S}^{(\tau)} = \{x \in R^3 \mid \exists \tilde{x} \in \partial S, \|x - \tilde{x}\| \leq \tau\}$ denote the border region of the expert annotation mask and the segmentation surface at tolerance τ , respectively. In this paper, we set the tolerance τ as 2.

Performance distribution of 86 internal validation tasks (DSC score)



Performance distribution of 60 external validation tasks (DSC score)



Context: Partial volume effect VS segmentation

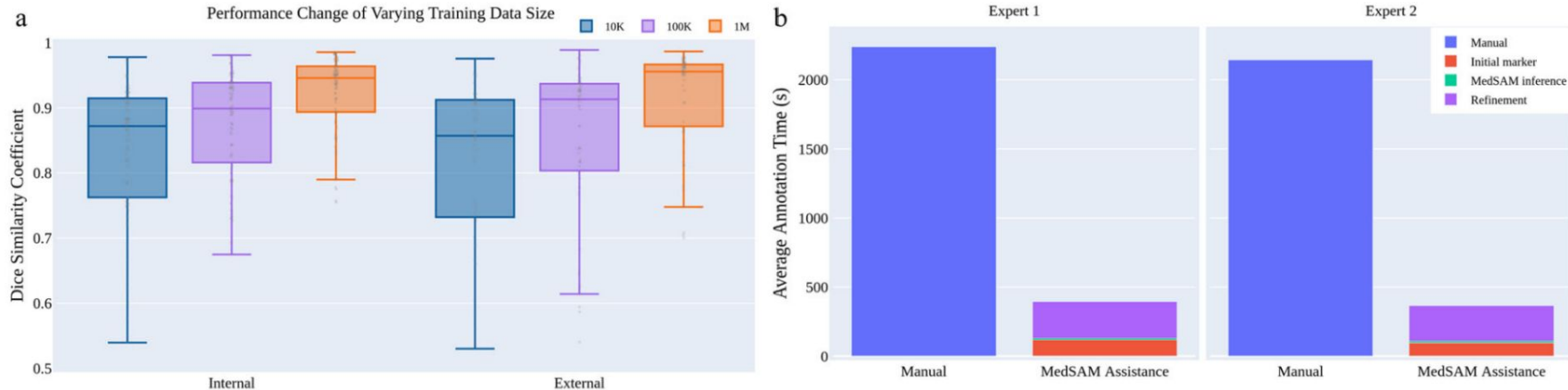


Fig. 5 | The effect of training dataset size and a user study of tumor annotation efficiency. a Scaling up the training image size to one million can significantly improve the model performance on both internal and external validation sets.

b MedSAM can be used to substantially reduce the annotation time cost. Source data are provided as a Source Data file.

- Linear marker every 3-10 slices by two experts, before MedSAM segmentation, and expert revision (3D adrenal tumors)
- Annotation time reduced by 82.37% and 82.95% for the two experts respectively

Some external validation on MRIs (DSC and NSD)



Fig. 11. Box plots of dice similarity coefficient and normalized surface distance scores for each MR segmentation task in external validation. The center line within the box represents the median value, with the bottom and top bounds of the box delineating the 25th and 75th percentiles, respectively. Whiskers are chosen to show the 1.5 of the interquartile range. Source data are provided as a Source Data file.

Discussion

Limitations:

- **Modality imbalance in the training set:** underperform on less-represented modalities
- **Bounding box prompt can be ambiguous** for segmentation of vessel-like branching structures

Conclusion:

- Holds great potential to accelerate the advancement of new diagnostic and therapeutic tools



Thank you for your attention

Context: Partial volume effect VS segmentation

Discussion